AFRL-AFOSR-VA-TR-2021-0060

Development of Beta Gallium Oxide on Large Area Substrates

Speck, James
UNIVERSITY OF CALIFORNIA SANTA BARBARA
3227 CHEADLE HL
SANTA BARBARA, CA,
US

06/27/2021
Final Technical Report

DISTRIBUTION A: Distribution approved for public release.

Air Force Research Laboratory
Air Force Office of Scientific Research
Arlington, Virginia 22203
Air Force Materiel Command

REPORT DOCUMENTATION PAGE			*Form Approved* *OMB No. 0704-0188*

The public reporting burden for this collection of information is estimated to average 1 hour per response, including the time for reviewing instructions, searching existing data sources, gathering and maintaining the data needed, and completing and reviewing the collection of information. Send comments regarding this burden estimate or any other aspect of this collection of information, including suggestions for reducing the burden, to Department of Defense, Washington Headquarters Services, Directorate for Information Operations and Reports (0704-0188), 1215 Jefferson Davis Highway, Suite 1204, Arlington, VA 22202-4302. Respondents should be aware that notwithstanding any other provision of law, no person shall be subject to any penalty for failing to comply with a collection of information if it does not display a currently valid OMB control number.
PLEASE DO NOT RETURN YOUR FORM TO THE ABOVE ADDRESS.

1. REPORT DATE *(DD-MM-YYYY)*	**2. REPORT TYPE**	**3. DATES COVERED** *(From - To)*
27-06-2021	Final	08 Dec 2017 - 07 Dec 2020

4. TITLE AND SUBTITLE Development of Beta Gallium Oxide on Large Area Substrates	**5a. CONTRACT NUMBER**
	5b. GRANT NUMBER FA9550-18-1-0059
	5c. PROGRAM ELEMENT NUMBER 61102F
6. AUTHOR(S) James Speck	**5d. PROJECT NUMBER**
	5e. TASK NUMBER
	5f. WORK UNIT NUMBER
7. PERFORMING ORGANIZATION NAME(S) AND ADDRESS(ES) UNIVERSITY OF CALIFORNIA SANTA BARBARA 3227 CHEADLE HL SANTA BARBARA, CA US	**8. PERFORMING ORGANIZATION REPORT NUMBER**
9. SPONSORING/MONITORING AGENCY NAME(S) AND ADDRESS(ES) AF Office of Scientific Research 875 N. Randolph St. Room 3112 Arlington, VA 22203	**10. SPONSOR/MONITOR'S ACRONYM(S)** AFRL/AFOSR RTB1
	11. SPONSOR/MONITOR'S REPORT NUMBER(S) AFRL-AFOSR-VA-TR-2021-0060

12. DISTRIBUTION/AVAILABILITY STATEMENT
A Distribution Unlimited: PB Public Release

13. SUPPLEMENTARY NOTES

14. ABSTRACT
In this program, we have explored high-quality homoepitaxy growth with ß-Ga2O3 using conventional PAMBE and MOCATAXY on different crystal orientations, and MOCVD (with Agnitron Collaboration) for high-mobility epitaxial films. We have also developed device design and processing with ß-Ga2O3 for high-power applications.

15. SUBJECT TERMS

16. SECURITY CLASSIFICATION OF:			**17. LIMITATION OF ABSTRACT**	**18. NUMBER OF PAGES**	**19a. NAME OF RESPONSIBLE PERSON**
a. REPORT	**b. ABSTRACT**	**c. THIS PAGE**			ALI SAYIR
U	U	U	UU	11	**19b. TELEPHONE NUMBER** *(Include area code)* 426-7236

Standard Form 298 (Rev.8/98)
Prescribed by ANSI Std. Z39.18

Final Report to

Dr. Ali Sayir
AF OFFICE OF SCIENTIFIC RESEARCH
875 NORTH RANDOLPH STREET, RM 3112
ARLINGTON VA 22203
ali.sayir.2@us.af.mil

Development of Beta Gallium Oxide on Large Area Substrates

AFOSR Award Number: FA9550-18-1-0059

by

James S. Speck
Materials Department
University of California
Santa Barbara, CA 93106
speck@ucsb.edu

DISTRIBUTION A: Distribution approved for public release.

Materials and Devices with β-Ga_2O_3

In this program, we explored high-quality homoepitaxy growth with β-Ga_2O_3 using conventional PAMBE and MOCATAXY on different crystal orientations, and MOCVD (with Agnitron Collaboration) for high-mobility epitaxial films. We have also developed device design and processing with β-Ga_2O_3 for high-power applications.

1. Material Development

(i) MBE Growth and Metal Oxide Catalyzed Epitaxy (MOCATAXY)

We have studied the MBE growth of β-Ga_2O_3 and β-$(Al_xGa_{1-x})_2O_3$ via conventional MBE growth, and via metal oxide catalyzed epitaxy (MOCATAXY), which shows the ability to markedly improve growth rates and material quality in MBE growth. We showed that MOCATAXY growth, which uses an additional indium flux as a catalyst during MBE growth, can expand the range of growth temperatures that (010) β-$(Al_xGa_{1-x})_2O_3$ can grow up to 900 °C, without sacrificing material quality. Additionally, minimal indium incorporation was measured in the film by APT, and clear thickness fringes were observed in XRD as shown in Fig. 1a. [1]

MOCATAXY growth was also expanded to other orientations, showing the ability to improve growth rates and allow for growth at much higher temperatures in (010) and (001) β-Ga_2O_3. (001) β-Ga_2O_3 in particular had been limited by lower growth rates due to increased suboxide desorption during conventional PAMBE growth in this orientation. MOCATAXY helps limit this suboxide desorption and allows for approximately 5 times the growth rate of conventional PAMBE for (001) β-Ga_2O_3. A summary of growth rates for various orientations is shown in Fig. 1b. [2]

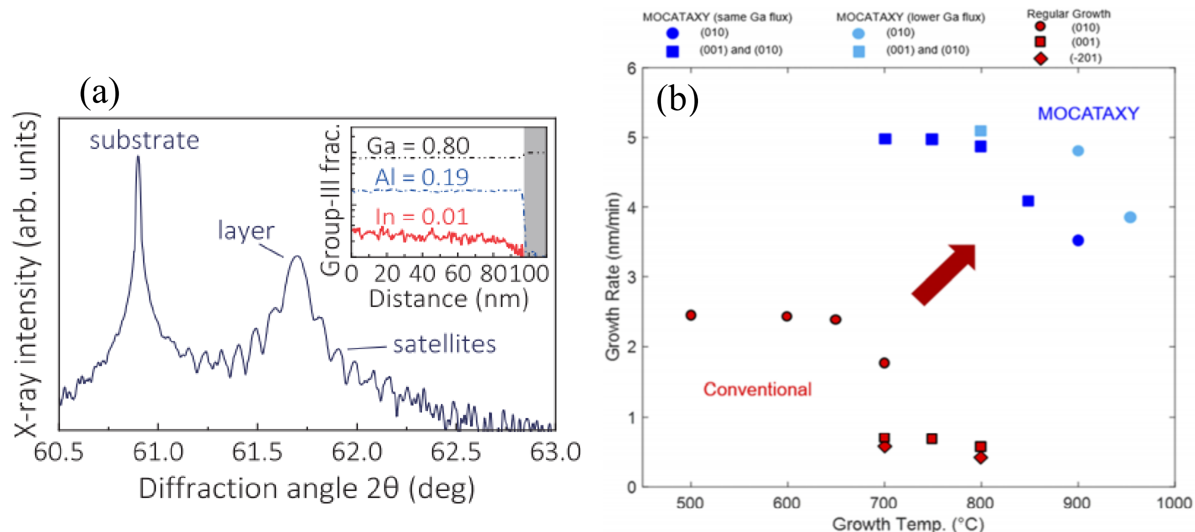

Fig. 1. (a) β-$(Al_xGa_{1-x})_2O_3$ XRD scan showing thickness fringes and a high intensity (020) β-$(Al_xGa_{1-x})_2O_3$ peak indicative of thickness and compositional uniformity. APT shows relatively low indium incorporation in the film. (b) Comparison of maximum growth rates achieved for various growth temperatures and crystallographic orientations for conventional PAMBE and MOCATAXY.

DISTRIBUTION A: Distribution approved for public release.

Room temperature Hall mobilities for (001) β-Ga_2O_3 films were also significantly higher for MOCATAXY grown films, further showing promise for this catalytic growth to allow for future (001) β-Ga_2O_3 devices. [2]

(ii) Doping

Sn doping via conventional PAMBE and MOCATAXY growth has been studied in detail. For conventional PAMBE of (010) β-Ga_2O_3, higher Sn doping concentrations were achievable, however the lower Sn cell temperatures needed to achieve the lower doping range, resulted in inconsistent Sn doping profiles. Both significant doping delay at the start of a doping profile, as well as surface segregation after the Sn shutter was closed were observed in SIMS profiles. MOCATAXY growth, on the other hand, allowed for sharp controllable profiles over a wide range of concentrations (10^{16} cm^{-3} to 10^{19} cm^{-3}). A relatively high room temperature mobility of 132 cm^2/Vs was achieved for a carrier concentration of 4 x 10^{16} cm^{-3} in a MOCATAXY grown (010) β-Ga_2O_3 film. [3]

Temperature dependent Hall measurement on a Sn doped (010) β-Ga_2O_3 film revealed a Sn donor level at 77 meV below the conduction band. At lower temperatures, maximum Hall mobility was limited, likely due to ionized impurity scattering due to a high background impurity concentration in the film. Temperature dependent Hall mobility and carrier concentration are shown in Fig. 2a. [3]

In additional to studying intentional n-type doping in MBE, unintentional Fe incorporation into films from Fe doped substrates was investigated. The observed Fe tail into epitaxially grown films was determined to be a result of a temperature dependent surface segregation effect, rather than diffusion. This effect led to an Fe tail observed in SIMS, with the length of this tail increasing for higher growth temperatures. Fig. 1b shows SIMS profiles demonstrating this effect as Fe incorporates more readily at lower growth temperatures, allowing for faster trapping of this total surface riding Fe, thereby limiting the length of this Fe tail into the film. Growing a low

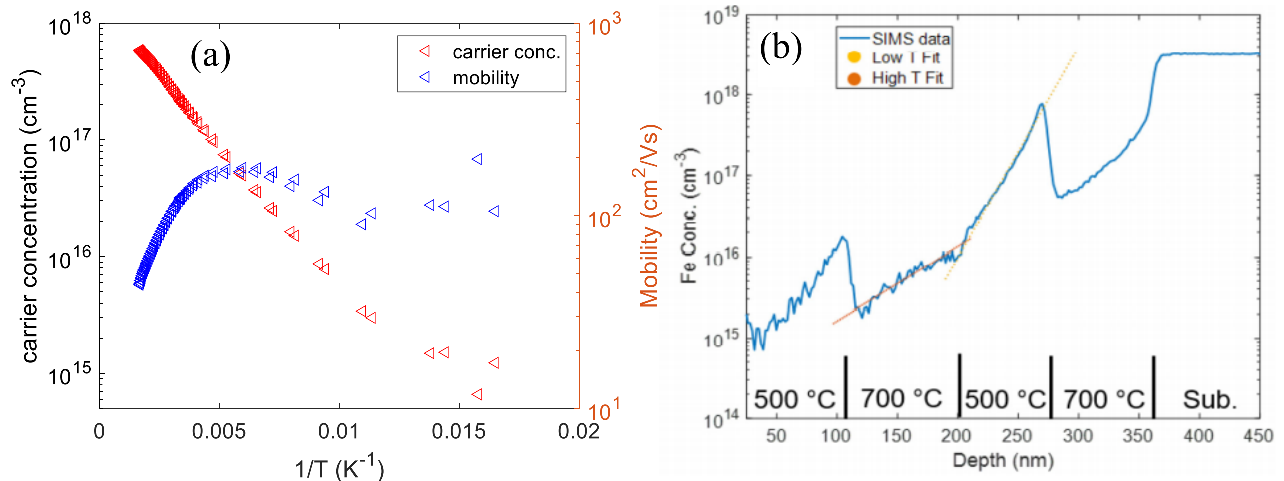

Fig. 2. (a) Temperature dependent Hall carrier concentration and mobility of Sn doped (010) β-Ga_2O_3 film. (b) Fe incorporation into the MBE grown film measured by SIMS for a film structure with varying growth temperatures.

DISTRIBUTION A: Distribution approved for public release.

temperature, Fe trapping buffer layer prior to active regions of devices structures was determined to be a solution to the problem of unintentional compensation in devices due to this Fe incorporation. [4]

(iii) (110) Growth Orientation

We explored the epitaxial growth of β-Ga_2O_3 on Sn-doped (110) substrates via PAMBE. The AFM scan of the as-received (110) substrates shows a very low RMS roughness of 0.08 nm for its smooth surface. Additionally, the result of miscut measurement shows that the miscut angle along the [001] direction and [201] direction is 0.1°. For the substrate polishing procedure, RHEED measurement reveals the existence of crystallographically equivalent (110) and (-110) facets on (010) substrate after Ga polishing by confirming chevron patterns, while there were only streaky patterns on (110) substrate indicative of smooth surface morphology as shown in Fig. 3a.[5]

Growth characteristics of β-Ga_2O_3 grown on (110) substrates at different Ga fluxes and substrate temperatures were studied in detail. From XRD rocking curve scan, the FWHM of the (110) peak is ~41 arc sec, which is comparable to the values reported for epitaxial films grown on (010) substrates. The trend of growth rate is nearly the same between β-Ga_2O_3 epitaxial films grown on (110) and (010) substrates. However, the growth rate on (110) substrates in the plateau region is 10% lower than that of (010) substrate as shown in Fig. 3b. This could be attributed to the geometry of the inclined (110) facets in (010) growth, the exposed (110) surface area is ~10% more than that of (110) growth. Furthermore, the surface morphology of β-Ga_2O_3 epitaxial films is smooth on both (110) and (010) substrates with RMS roughness around 1.0 nm. Additionally, elongated features oriented along the [001] direction are exhibited in the plateau regime on both (110) and (010) substrates, while this feature is not expected on the films grown on the (110) substrates due to the absence of clear faceting. Despite the appearance of (110) facets in the growth of (010) β-Ga_2O_3, the (110) plane does not have a tendency to show a well-defined step–terrace structure.

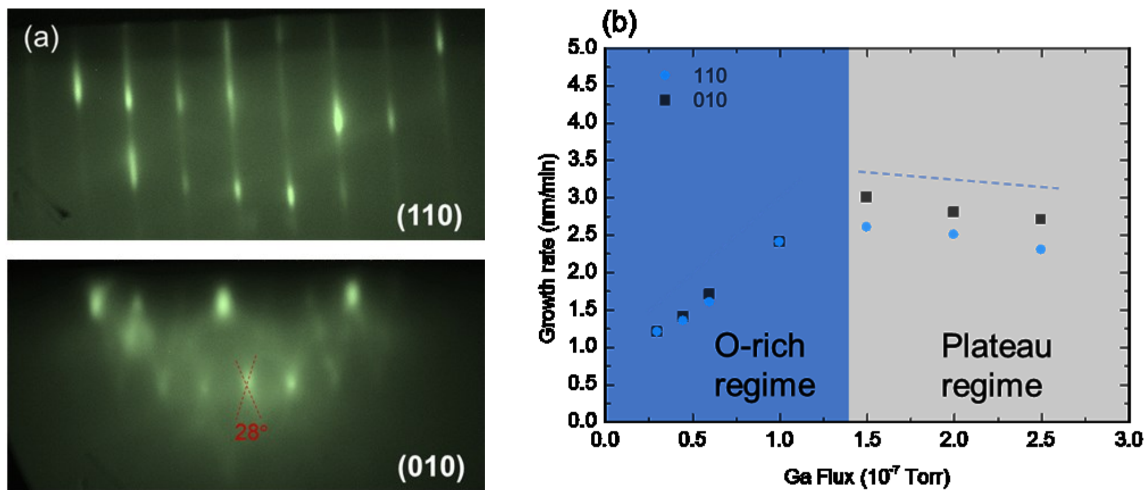

Fig. 3. (a) RHEED patterns of (110) substrates and (010) substrates after 10 min Ga polishing. (b) Growth rates of β-Ga2O3 epitaxial films grown on (110) and (010) substrates at 700 °C.

DISTRIBUTION A: Distribution approved for public release.

(iv) MOCVD grown β-Ga_2O_3

In collaboration with Agnitron Technology we have also worked on characterization of MOCVD grown β-Ga_2O_3. Temperature dependent Hall measurements were performed on lightly doped n-type MOCVD grown films to achieve a room temperature mobility of 176 cm^2/Vs, a demonstration that first showed the ability of MOCVD films to provide device quality mobility necessary for vertical structures for high field applications. Highly Sn doped n+ contacts were grown via MBE to allow for ohmic contact at the low temperatures of the Hall measurement. [6] Since then, demonstration of extremely high low temperature mobility exceeding 10^4 cm^2/Vs [7] and room temperature carrier concentrations of low 10^{14} cm^{-3} [8] have been achieved, showing the high purity and low carrier concentrations necessary for efficient vertical high field devices. Work on this material will be discussed later in this review.

References

[1] P. Vogt, A. Mauze, F. Wu, B. Bonef, and J. S. Speck. Appl. Phys. Exp. **11**, 115503 (2018).
[2] A. Mauze, Y. Zhang, T. Itoh, F. Wu, and J. S. Speck. APL Materials **8**, 021104 (2020).
[3] A. Mauze, Y. Zhang, T. Itoh, E. Ahmadi, J.S. Speck. Appl. Phys. Lett. **117**, 222102 (2020).
[4] A. Mauze, Y. Zhang, T. Mates, F. Wu, and J.S. Speck. **115**, 052102 (2019).
[5] T. Itoh, A. Mauze, Y. Zhang. J. S. Speck. Appl. Phys. Lett. **117**, 152105 (2020).
[6] Y. Zhang, F. Alema, A. Mauze, O.S. Koksaldi, R. Miller, A. Osinsky, and J.S. Speck. APL Mat. **7,** 022506 (2019).
[7] F. Alema, Y. Zhang, A. Osinsky, N. Valente, A. Mauze, T. Itoh, and J.S. Speck. APL Mat. **7**, 121110 (2019).
[8] F. Alema, Y. Zhang, A. Osinsky, N. Orishchin, N. Valente, A. Mauze, and J.S. Speck. APL Mat. **8**, 021110 (2020).

2. High-power Device Development

(i) Anisotropic Wet Etch of β-Ga_2O_3

We have developed anisotropic wet-etch processing of β-Ga_2O_3 with hot H_3PO_4 (120-160 °C) that can enable dry-etch damage removal and development of submicron channels for FinFETs. A systematic study was performed on a fabricated wagon wheel pattern on β-Ga_2O_3 (010) substrate that showed a directional dependence of β-Ga_2O_3 etch by hot H_3PO_4, [1] with the [001] direction revealing faster etch rate and near vertical profile as shown in Fig. 4a.

A further evaluation of this wet-etch process was performed on sidewall Schottky diodes fabricated on MOCVD (010) β-Ga_2O_3 films on Fe-doped substrates. [2] The wet-etched Schottky diodes showed superior characteristics with near unity ideality factor and reduced hysteresis compared to the ones without wet-etch as shown in Figs. 4b and 4c. This wet-etch method appears to be a useful technique for low-damage and ultra-scaled device that was used in our subsequent FINFET development.

DISTRIBUTION A: Distribution approved for public release.

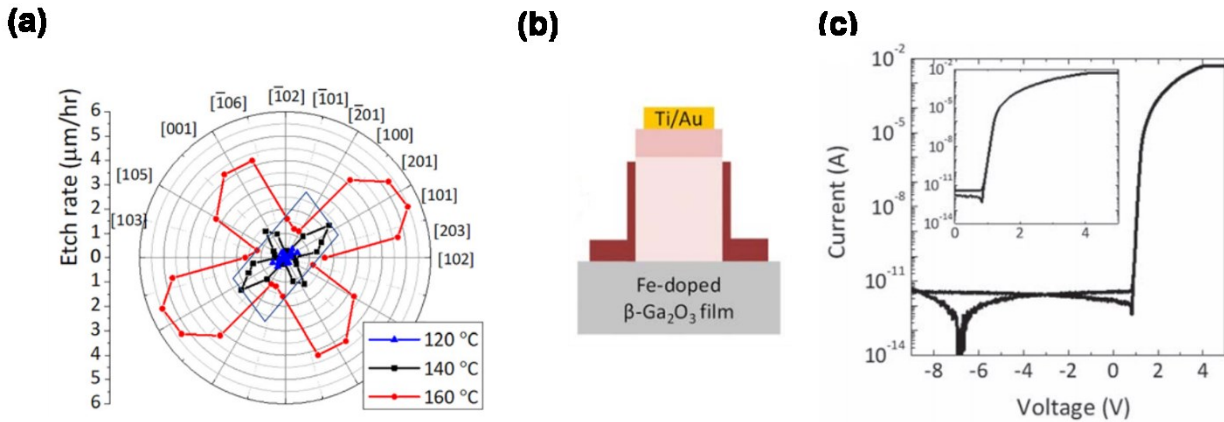

Fig. 4. (a) β-Ga_2O_3 sidewall etch rate at different H_3PO_4 temperatures. [1] Higher etch rates are obtained near the [001] and [201] directions, and sidewall Schottky diode with wet-etch (b) fabricated device structure, and (c) current-voltage characteristics with unity ideality factor and no hysteresis. [2]

(ii) Lateral FINFETs

We developed lateral Fin transistors with both MISFETs and MESFET structures on MOCVD (010) β-Ga_2O_3 on Fe-doped substrates using the wet-etch technique with hot H_3PO_4. [3] The devices had fin length of 3 μm, gate length of 1 μm, gate–source spacing of 5 μm, and gate–drain spacing of 9 μm. The FINFET devices comprised of uniformly distributed 72 fins with a total width of 200 μm. The breakdown voltage of the MESFET was obtained as 1263 V whereas the MISFET demonstrated a breakdown voltage of 787 V as shown in Fig. 5.

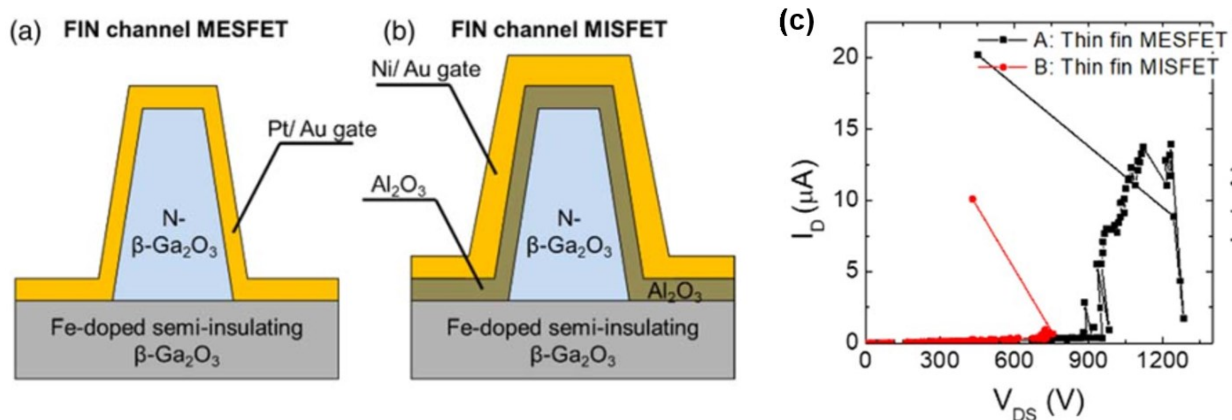

Fig. 5. MOCVD (010) β-Ga_2O_3 (a) MESFET, (b) MISFET, and (c) breakdown characteristics [3].

(iii) Vertical Field-plate Schottky Diodes

We also developed vertical field-plate Schottky barrier diodes using MOCVD (010) β-Ga_2O_3 since vertical devices offer superior power handling capability and scaling feasibility compared to the lateral ones. The Schottky diodes consisted of nominal ~1.1 μm lightly Si-doped n− β-Ga_2O_3

DISTRIBUTION A: Distribution approved for public release.

drift layer (~low 10^{16} cm^{-3} doping) grown on a 0.2 μm n^+ buffer layer ([Si]~5×0^{18} cm^{-3}) on top of a Sn-doped substrate. [4] The field-plate Schottky diodes exhibited a low differential specific on-resistance of 0.67 mΩ-cm^2, a punch-through breakdown voltage of 165 V, and a higher Baliga's figure of-merit (BFOM) compared to the devices from other growth methods of similar drift layer thickness (Fig. 6). The low $R_{on,sp}$ can be potentially contributed from the high-mobility MOCVD β-Ga_2O_3 drift layer. Our results suggest the MOCVD β-Ga_2O_3, with higher mobility and background impurity, can be promising for high-power vertical devices.

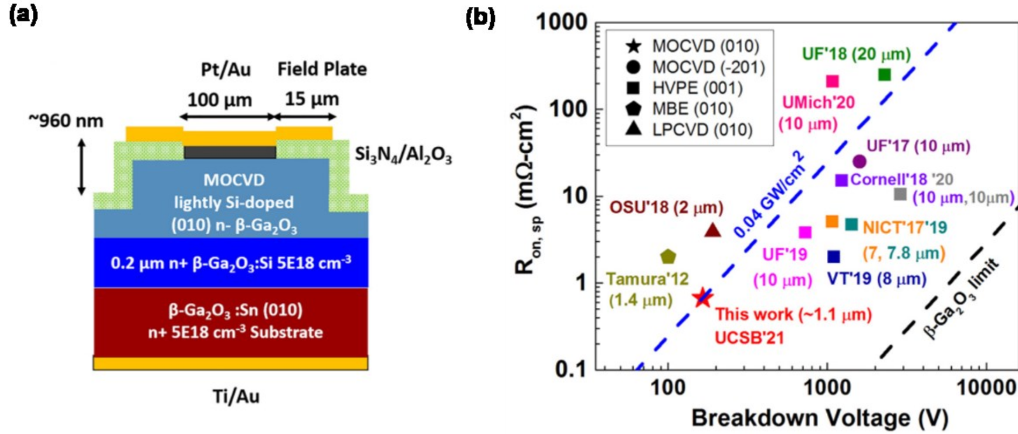

Fig. 6. (a) MOCVD β-Ga_2O_3 vertical field-plate Schottky diodes, (b) $R_{ON,sp}$ versus breakdown voltage of vertical β-Ga_2O_3 Schottky diodes from our work and from prior reports (drift layer thickness shown in parenthesis). [4] Our devices provided better BFOM compared to similar thickness devices by other growth methods, such as LPCVD (OSU'18) and MBE (Tamura'12).

(iv) Power Device Figure-of-Merit

We have evaluated the potential of β-Ga_2O_3 for high-power application revisiting the power device figure-of-merit. The conventional BFOM considers complete dopant ionization in the evaluation of on-resistance. However, in UWBG semiconductors, this is often not the case as the shallow dopants transform to deep levels providing only partial ionization, and are often compensated by impurities. The β-Ga_2O_3 offers an additional advantage here with a wide range of shallow dopants available (Si, Ge, Sn), their high ionization efficiency, and high-material purity compared to other UWBG semiconductors (e.g. AlN and diamond). With the actual material expectations included in terms of dopant ionization and impurity compensation effects, β-Ga_2O_3 showed a superior "Modified BFOM" compared to other UWBG semiconductors as shown in Fig 7. [5]

DISTRIBUTION A: Distribution approved for public release.

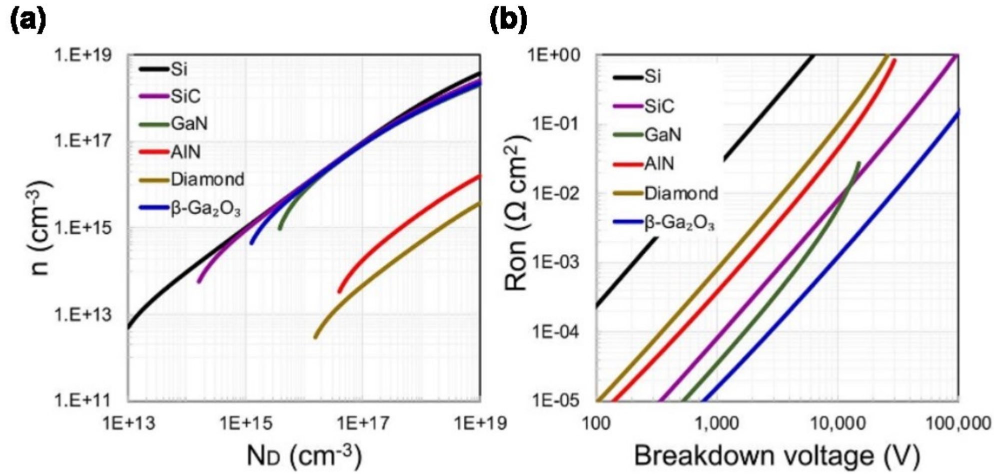

Fig 7. (a) Ionized doping in different semiconductors with respect to the background doping considering compensation effects by acceptor-like impurities. (b) Modified BFOM contour showing β-Ga_2O_3 can provide higher BFOM compared to other UWBG semocnductors when material purity and dopant ionization effieceny are considered to estimate BFOM. [5]

3. Application of β-Ga_2O_3 Devices in Harsh Environment

To investigate β-Ga_2O_3 device performance in harsh radiation application, we explored neutron radiation effects in UCSB-grown PAMBE Ge-doped β-Ga_2O_3 epitaxy and EFG-grown UID substrates from Tamura using Ni/β-Ga_2O_3 Schottky diodes. [6, 7] The samples were irradiated together at the Ohio State University Research Reactor (OSURR) for a fair comparison. Each sample was diced into two pieces in order to separately irradiate them with two different fluences of fast neutrons (>0.5 eV) with exposure time of 30 and 60 minutes at 450 kW in OSURR that provided a 1 MeV neutron equivalent fluence as 8.5×10^{14} cm^{-2} and 1.7×10^{15} cm^{-2}, respectively.

After the radiation, the irradiated PAMBE β-Ga_2O_3 diodes revealed a carrier removal rate of ~19 ± 0.3 cm^{-1} which was ~2.7 times lower compared to the ones on EFG-grown substrate with a carrier removal rate of ~51 ± 3.5 cm^{-1} (Fig. 8a). Moreover, a prior work on SiC Schottky diodes irradiated in the same OSURR reactor revealed a carrier removal rate of ~48.5 ± 6.3 cm^{-1} (Fig. 8b). Our work revealed PAMBE β-Ga_2O_3 to be ~2.5 times more radiation hard compared to SiC which will be promising for MBE β-Ga_2O_3 devices for extreme environment applications. [7]

DISTRIBUTION A: Distribution approved for public release.

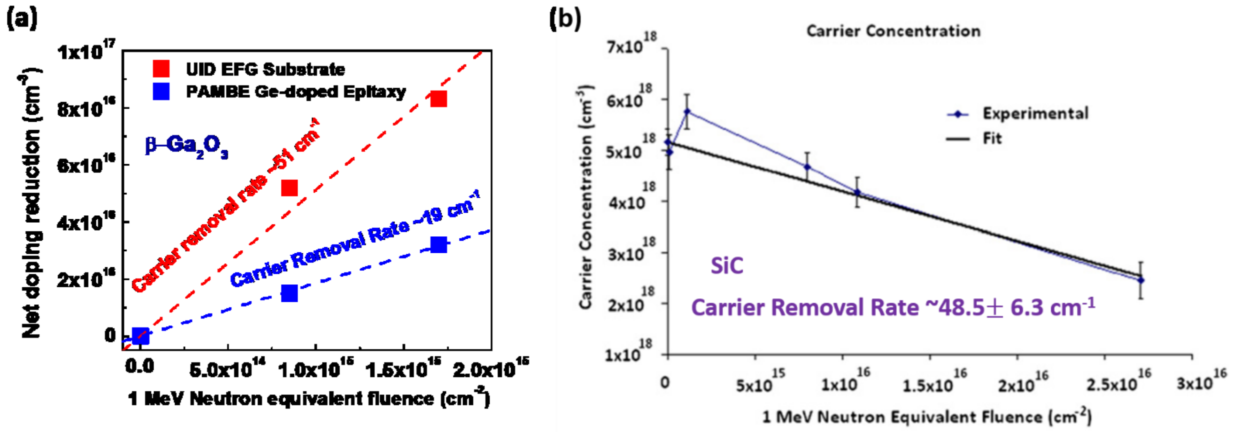

Fig. 8- Carrier removal rate in neutron-irradiated samples (a) β-Ga_2O_3 EFG substrate and PAMBE epitaxy [6, 7], (b) SiC [8] showing PAMBE β-Ga_2O_3 has ~2.5 times less carrier removal rate compared to SiC.

References

[1] Y. Zhang, A. Mauze, and J. S. Speck, *Appl. Phys. Lett.* **115**, 013501 (2019).
[2] Y. Zhang, A. Mauze, F. Alema, A. Osinsky, and J. S. Speck, *Appl.Phys. Express* **12**, 044005 (2019).
[3] Y. Zhang, A. Mauze, F. Alema, A. Osinsky, T. Itoh, and J. S. Speck, *J. J. of Appl. Phys.* **60**, 014001 (2021).
[4] E. Farzana, F. Alema, W. Y. Ho, A. Mauze, T. Itoh, A. Osinsky, and J. S. Speck, *Appl. Phys. Lett.* **118**, 162109 (2021).
[5] Y. Zhang and J. S. Speck, *Semicond. Sci. Technol.* **35**, 125018 (2020).
[6] E. Farzana, M. Chaiken, T. Blue, A. R. Arehart, and S. A. Ringel, *APL Materials* **7**, 022502 (2019).
[7] E. Farzana**,** A. Mauze, J. B. Varley, J. S. Speck, A. R. Arehart, and S. A. Ringel, *APL Materials* **7**, 121102 (2019).
[8] E. Almaz, S. Stone, T. E.Blue, and J. P. Heremans, *Nucl. Inst. and Methods in Phy. Res A* **622**, 200 (2010).

3. Density Functional Theory

In collaboration with the Chris Van de Walle group at UCSB, we have explored the properties of Ga_2O_3 alloys and acceptor dopant diffusion via hybrid density functional theory. For the Al_2O_3-Ga_2O_3 alloy system, it was determined that the monoclinic crystal structure was preferred for Al contents up to 71%. The conduction band and valence band offsets were calculated between Al_2O_3 and Ga_2O_3 for the monoclinic and corundum structures. Additionally, valence and conduction band offsets were calculated for the β-$(Al_xGa_{1-x})_2O_3$/Ga_2O_3 heterostructure as a function of Al content x as shown in Fig. 9. [1] Achieving high Al content to obtain high conduction band offsets is necessary to produce high 2DEG densities for efficient modulation doped field effect transistors in the future.

DISTRIBUTION A: Distribution approved for public release.

Investigation into diffusion of the deep acceptors Mg and N was performed as well. Here it was found that Mg can incorporate on the Ga site as a deep acceptor or on the O site as a deep donor. N can incorporate on the O site as a deep acceptor, but can also incorporate on the Ga site. Mg was shown to diffuse rapidly as an interstitial in a process that is assisted by Ga interstitials. N diffusion on the other hand is assisted by O vacancies. Mg diffusion occurs at significantly lower activation energies than N, suggesting it will diffuse at lower temperatures than N. [2]

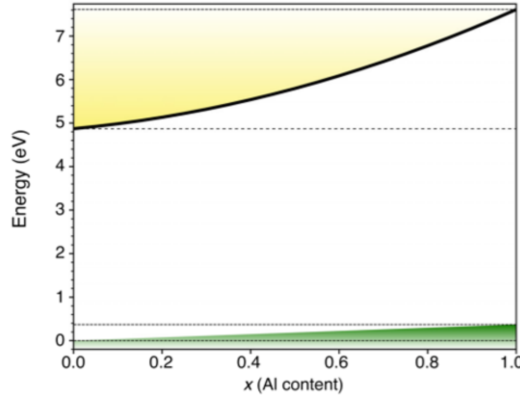

Fig. 9- Prediction of conduction and valence band offsets as a function of Al composition in β-$(Al_xGa_{1-x})_2O_3$, with β-Ga_2O_3 shown as the dotted lines.

References

[1] H. Peelaers, J.B. Varley, J.S. Speck, and C.G. Van de Walle. Appl. Phys. Lett. **112**, 242101 (2018).

[2] H. Peelaers, J.L. Lyons, J.B. Varley, and C.G. Van de Walle. APL Materials. **7** 022519 (2019).

DISTRIBUTION A: Distribution approved for public release.

All publications acknowledging award FA9550-18-1-0059

1. P. Vogt, A. Mauze, F. Wu, B. Bonef, and J. S. Speck. Appl. Phys. Exp. **11**, 115503 (2018). https://doi.org/10.7567/APEX.11.115503
2. H. Peelaers, J.B. Varley, J.S. Speck, and C.G. Van de Walle. Appl. Phys. Lett. **112**, 242101 (2018). https://doi.org/10.1063/1.5036991
3. Y. Zhang, F. Alema, A. Mauze, O.S. Koksaldi, R. Miller, A. Osinsky, and J.S. Speck. APL Mat. **7,** 022506 (2019). https://doi.org/10.1063/1.5058059
4. H. Peelaers, J.L. Lyons, J.B. Varley, and C.G. Van de Walle. APL Materials. **7** 022519 (2019). https://doi.org/10.1063/1.5063807
5. E. Farzana, M. Chaiken, T. Blue, A. R. Arehart, and S. A. Ringel, *APL Materials* **7**, 022502 (2019). https://doi.org/10.1063/1.5054606
6. F. Alema, B. Hertog, P. Mukhopadhyay, Y. Zhang, A. Mauze, A. Osinsky, W.V. Schoenfeld, J.S. Speck, and T. Vogt. APL Mat. **7**, 022527 (2019). https://doi.org/10.1063/1.5064471
7. Y. Zhang, A. Mauze, F. Alema, A. Osinsky, and J. S. Speck, *Appl. Phys. Express* **12**, 044005 (2019). https://doi.org/10.7567/1882-0786/ab08ad
8. M. Hilfiker, U. Kilic, A. Mock, V. Darakchieva, S. Knight, R. Korlacki, A. Mauze, Y. Zhang, J.S. Speck, M. Schubert. Appl. Phys. Lett. **114,** 231901 (2019). https://doi.org/10.1063/1.5097780
9. Y. Zhang, A. Mauze, and J. S. Speck, *Appl. Phys. Lett.* **115**, 013501 (2019). https://doi.org/10.1063/1.5093188
10. A. Mauze, Y. Zhang, T. Mates, F. Wu, and J.S. Speck. **115**, 052102 (2019). https://doi.org/10.1063/1.5096183
11. E. Farzana**,** A. Mauze, J. B. Varley, J. S. Speck, A. R. Arehart, and S. A. Ringel, *APL Materials* **7**, 121102 (2019). https://doi.org/10.1063/1.5126463
12. F. Alema, Y. Zhang, A. Osinsky, N. Valente, A. Mauze, T. Itoh, and J.S. Speck. APL Mat. **7**, 121110 (2019). https://doi.org/10.1063/1.5132954
13. F. Alema, Y. Zhang, A. Osinsky, N. Orishchin, N. Valente, A. Mauze, and J.S. Speck. APL Mat. **8**, 021110 (2020). https://doi.org/10.1063/1.5132752
14. A. Mauze, Y. Zhang, T. Itoh, F. Wu, and J. S. Speck. APL Materials **8**, 021104 (2020). https://doi.org/10.1063/1.5135930
15. C. Yuan, Y. Zhang, R. Montgomery, S. Kim, J. Shi, A. Mauze, T. Itoh, J.S. Speck, and S. Graham. J. Appl. Phys. **127**, 154502 (2020). https://doi.org/10.1063/1.5141332
16. F. Alema, Y. Zhang, A. Mauze, T. Itoh, J.S. Speck, B. Hertog, and A. Osinsky. AIP Advances **10**, 085002 (2020). https://doi.org/10.1063/5.0011910
17. T. Itoh, A. Mauze, Y. Zhang. J. S. Speck. Appl. Phys. Lett. **117**, 152105 (2020). https://doi.org/10.1063/5.0027884
18. A. Mauze, Y. Zhang, T. Itoh, E. Ahmadi, J.S. Speck. Appl. Phys. Lett. **117**, 222102 (2020). https://doi.org/10.1063/5.0027870
19. Y. Zhang and J. S. Speck, *Semicond. Sci. Technol.* **35**, 125018 (2020). https://doi.org/10.1088/1361-6641/abbba6
20. Y. Zhang, A. Mauze, F. Alema, A. Osinsky, T. Itoh, and J. S. Speck, *J. J. of Appl. Phys.* **60**, 014001 (2021). https://doi.org/10.35848/1347-4065/abcf05
21. E. Farzana, F. Alema, W. Y. Ho, A. Mauze, T. Itoh, A. Osinsky, and J. S. Speck, *Appl. Phys. Lett.* **118**, 162109 (2021). https://doi.org/10.1063/5.0047821

DISTRIBUTION A: Distribution approved for public release.